PLANT SCIENCE TODAY
Vol x(x): xx–xx
https://doi.org/10.14719/pst.14273

eISSN 2348-1900

RESEARCH ARTICLE

In silico evaluation of *Ulex europaeus* L. phytochemicals for identification of potential inhibitors against Marburg virus viral protein 24

Shreya Joshi[1], Deependra Joshi[1], Hasanain A J Gharban[2], Bhawana Yadav[1], Shiva Prasad Kollur[3], P Saranraj[4], Madhulika Esther Prasad[5], Vijay Jagdish Upadhye[6*] & Pallavi Singh[1*]

[1]Department of Biotechnology, Graphic Era (Deemed to be University), Dehradun 248 002, Uttarakhand, India
[2]Department of Internal and Preventive Veterinary Medicine, College of Veterinary Medicine, University of Wasit, Wasit 52001, Iraq
[3]School of Physical Sciences, Amrita Vishwa Vidyapeetham, Mysuru 570 026, Karnataka, India
[4]Department of Microbiology, Sacred Heart College (Autonomous), Tirupattur 635 601, Tamil Nadu, India
[5]Department of Biochemistry and Biotechnology, School of Life Sciences, Sardar Bhagwan Singh University, Dehradun 248 019, Uttarakhand, India
[6]Research and Development cell, Parul Institute of Applied Sciences (PIAS), Parul University, Vadodara 391 760, Gujarat, India

*Correspondence email - Dr.vijaysemilo@gmail.com; pallavisingh.bt@geu.ac.in

Received: 27 February 2026; Accepted: 24 April 2026; Available online: Version 1.0: 04 June 2026

Cite this article: Shreya J, Deependra J, Hasanain AJG, Bhawana Y, Shiva PK, Saranraj P, Madhulika EP, Vijay JU, Pallavi S. *In silico* evaluation of *Ulex europaeus* L. phytochemicals for identification of potential inhibitors against Marburg virus viral protein 24. Plant Science Today (Early Access). https://doi.org/10.14719/pst.14273

Abstract

Marburg virus (MARV), a member of the Filoviridae family, is a highly virulent agent that exhibits clinical features similar to those of viruses in the Rhabdoviridae family. Currently, no antiviral or vaccine therapies are approved for MARV-infected patients. This highlights the need to identify new antiviral compounds. With the rising concerns of drug resistance, costs and side effects of synthetic drugs, the use of natural products as an alternative source of antiviral compounds is a promising approach. In the current study, potent inhibitors of MARV viral protein 24 (VP24) protein (PDB ID: 4OR8) were identified using structure-based virtual screening of phytochemicals derived from *Ulex europaeus* L. A library of phytochemicals was created using the IMPPAT database, followed by molecular docking and molecular dynamics (MD) simulation studies of the complexes formed between the identified compounds and the target protein. The MARV VP24 protein is an important target for antiviral therapy because of its involvement in viral nucleocapsid formation. The compound Ulexone B showed the highest binding affinity of -9.9 kcal/mol to the MARV VP24 protein, compared to Ulexone A and Ulexone C, which showed similar binding affinities of -8.7 kcal/mol each. Molecular dynamics simulation studies of the complex of Ulexone B and the MARV VP24 protein showed stable complex dynamics, as indicated by the root mean square deviation (RMSD), root mean square fluctuation (RMSF) and solvent accessible surface area (SASA) profiles of the complex.

Keywords: antiviral potential; drug discovery; Marburg virus; molecular docking; *Ulex europaeus*

Introduction

Emerging and re-emerging viral diseases continue to pose serious threats to global public health. Among these pathogens, the Marburg virus (MARV) remains one of the most lethal human viruses. This virus is responsible for deadly diseases such as Marburg virus disease (MVD) (1). The absence of approved antiviral therapies for MVD necessitates the targeting of essential viral components to suppress infection. The Marburg virus belongs to the Filoviridae family. This family also includes the Ebola virus and these two viruses share many structural and functional similarities. MARV causes a deadly hemorrhagic fever with fatality rates of more than 24 % and reaching up to 88 % in certain cases (2). The MARV is reported to cause frequent epidemics, mainly in sub-Saharan African regions, with a fatality rate ranging from 24 % to 90 % (1). It was first recognised in 1967 during simultaneous outbreaks in Marburg and Frankfurt (Germany) and Belgrade (Serbia). It was reported in laboratory workers handling tissues from infected African green monkeys (*Cercopithecus aethiops*) imported from Uganda. On September 27, 2024, the Rwandan Ministry of Health announced the country's first Marburg outbreak. Most confirmed cases were among healthcare facilities in Kigali. Rwanda recorded 66 cases and 15 deaths during the outbreak (3). The Marburg virus is an enveloped, negative-sense RNA virus with a genome of approximately 19 kb in length that encodes seven structural proteins, namely, nucleoprotein (NP), viral proteins (viral protein 35, viral protein 40, viral protein 30, viral protein 24), glycoprotein (GP) and L-polymerase, which are necessary for replication and immune evasion (4). The viral protein (VP) 24 contributes to viral assembly, nucleocapsid formation and modulation of host immune responses, particularly by interfering with interferon signalling pathways (5). Similarly, VP40 dimers, VP30 transcriptional factors and VP35 nucleocapsids are responsible for various functions in the MARV and serve as potential targets for antiviral development. The VP30 accelerates the reporter gene activity by two times for viral replication and VP40 mediates the budding of viral proteins that are localised to

the cell membrane (6). Host factors such as C-type lectins, TIM-1 and Niemann–Pick C1 (NPC1) are critically involved in MARV entry and intracellular trafficking (7). Owing to the extreme biosafety requirements (BSL-4) associated with live MARV experimentation, *in silico* drug discovery approaches have become important for the preliminary screening of antiviral compounds. In parallel, plant-derived natural products represent a chemically diverse and biologically rich source of antiviral scaffolds and have been widely recognised as valuable starting points for modern drug discovery. In the present study, ten medicinal plants were selected for computational screening based on their documented ethnopharmacological use and reported biological activities, including antimicrobial, antiviral, anti-inflammatory and immunomodulatory effects (8). The ethanolic extract of *U. europaeus* L. exhibited the highest antioxidant activity and phenolic content. *Anaphalis busua* (Buch.-Ham. ex D.Don) DC. *Andrographis paniculata* (Burm.f.) Wall. ex Nees, *Cajanus cajan* (L.) Huth, *Hardwickia binate* Roxb., *Harrisonia perforate* (Blanco) Merr., *Maclura pomifera* (Raf.) C.K.Schneid., *Malus communis* Desf., *Petiveria alliacea* L., *Prunus persica* L. and *Ulex europaeus* L. are the plants that were selected for the current study. The ethanolic extract of *U. europaeus* exhibited the highest antioxidant activity and phenolic content (9). It has been reported that the stem of *A. paniculata* has the potential to block the protease and spike angiotensin-converting enzyme 2 (ACE2) interaction (IC_{50} 0.034–11.61 uM across Calu-3/Vero-E6 models) of severe acute respiratory syndrome coronavirus 2 (SARS-CoV-2), complemented by the cytokine modulation, which prevents the hyperinflammatory cascades in viral replication activity (RA) and RA-associated problems (10). The *H. perforata* has also been reported to give luteolin-rich extracts and 16-not limonoids. These selectively inhibit 11 beta-hydroxysteroid dehydrogenase type 1 (HSD1) while simultaneously suppressing spike protein-triggered mitogen-activated protein kinase (MAPK)/NOD like receptor family pyrin domain containing 3 (NLRP3) inflammasome activation. This significantly reduces interleukin 6 (IL-6)/IL-1beta in epithelial cells of the lung (11). The *M. pomifera* extracts cause inclusion due to specific disruption of hydroxybenzyl alcohol in human respiratory syncytial virus (hRSV) membrane fusion and attachment (EC_{50} 3.85 mg/mL, selective index > 10) (12). The *M. domestica* juices are polyphenol rich and are reported to demonstrate prophylactic efficacy against influenza A/B via enhanced natural killer (NK) cell activity along with a reduction in viral hemagglutination (13). Researchers prioritised Himalayan methanol extracts of *A. busua* for protein denaturation inhibition (IB_{50} 24.10 ug/mL) and DPPH scavenging, which mitigate oxidative bursts (14). Oxidative burst is a characteristic of persistent viral infections. Methanol extracts of *P. persica* bark show concentration-dependent suppression of lipopolysaccharide (LPS)-induced nuclear factor kappa B (NF-kB) p65 translocation and downstream proinflammatory cytokines (TNF-alpha, IL-6, IL-1beta) in BV2 microglia ($p < 0.01$) (15). The study discusses the potential of iso-flavonoids from the leaf of *C. cajan* to demonstrate anti-inflammatory activity through the suppression of cytokine cascades (TNF-alpha, IL-6) and NF-kB signalling (16). Inhibition of pro-inflammatory mediators by the production of prenylated isoflavonoids in elicited hairy root culture is portrayed as evidence. Bark methanol extracts from *P. persica* also exhibit concentration-dependent inhibition of LPS-induced NF-kB p65 nuclear translocation (20–200ug/mL; $p < 0.01$) with reduction of TNF-alpha, IL-6 and IL-1beta in BV2 microglia (15). The study focuses on the potential of isoflavonoids from the leaf of *C. cajan* to demonstrate anti-inflammatory activity through the suppression of cytokine cascades (TNF-alpha, IL-6) and NF-kB signalling (16). According to the documented medicinal properties of *A. paniculata,* related plants were selected and verified via the IMPPAT database using related species. These plants were chosen due to their high level of bioactive phytochemicals suitable for drug development (6). The present study is guided by the objective of evaluating whether a systematic *in silico* pipeline integrating virtual screening, molecular docking and molecular dynamics simulation can identify phytochemicals from *U. europaeus* as effective inhibitors of the MARV. Given that the VP24 protein of the MARV remains relatively underexplored as a therapeutic target, it is further assessed for its potential in identifying novel inhibitors. Therefore, the objective of this study is to identify a potential lead molecule from *U. europaeus* against the VP24 protein using an *in silico* approach.

Materials and Methods

Protein selection and preparation

The crystal structure of the MARV VP24 protein (PDB ID: 4OR8; resolution 2.65 Å) was obtained from the Research Collaboratory for Structural Bioinformatics (RCSB) protein data bank (https://www.rcsb.org/). The protein structure was checked for missing residues. The protein was further processed in BIOVIA Discovery Studio (v25.1.0.24284), which included the removal of heteroatoms and water molecules, followed by the addition of the polar hydrogen atom (17).

Phytochemical library generation

The Indian medicinal plants, phytochemistry and therapeutics (IMPPAT 2.0) database (https://cb.imsc.res.in/imppat/), a manually created database, was used to build the library of 207 phytochemicals. From the 10 selected plants, *A. busua*, *A. paniculata*, *C. cajan*, *H. binata*, *H. perforata*, *M. pomifera*, *M. communis*, *P. alliacea*, *P. persica* and *U. europaeus* were used for virtual screening (18). Phytochemicals that passed Lipinski's rule of five were downloaded. PubChem was used to retrieve the 3D structures of the selected phytochemicals in SDF format for further analysis. A library of 207 phytochemicals used in this study is provided in Supplementary Table 1 (19, 20).

Virtual screening and molecular docking of the selected phytochemicals

Molecular docking was performed using the PyRx 0.8 virtual screening tool, which examined the binding affinity of the different phytochemicals against the target protein (21). The ligand energies were minimised and converted to the protein data bank, partial charge and atom type (PDBQT) format. Molecular docking was performed with the following coordinates, X:54.35, Y:49.11 and Z:67.92 Å. Molecular docking values of 207 phytochemicals against target protein VP24 (PDB ID: 4OR8) are provided in Supplementary Table 2. The top 10 phytochemicals, which showed the highest binding affinities, were selected for further studies. Further, the amino acid residues involved in the interactions of the target protein with the top 3 docked ligands were analysed and visualised using BIOVIA Discovery Studio (v25.1.0.24284) (22).

Absorption, distribution, metabolism, excretion and toxicity analysis

The pharmacological and drug-like properties of the phytochemical compounds were evaluated using Swiss ADME (http://www.swissadme.ch/). The ADME allows users to evaluate parameters such as lipophilicity, water solubility, drug-like rules, pharmacokinetic properties and medicinal chemistry (23). Along with absorption, distribution, metabolism, excretion and toxicity (ADMET) parameters, the toxicity class of the phytochemicals, Ulexone A, Ulexone B and Ulexone C, was predicted by the ProTox3.0 (https://tox.charite.de/protox3/) tool (24).

Molecular dynamics simulations

Based on the molecular docking results, the complex of Ulexone B with target protein VP24 was subjected to molecular dynamics (MD) simulations. These simulations were performed using GROMACS 2024.2 to evaluate the structural stability and the influence of the ligand on the internal dynamics of the 4OR8 receptor.

Following the docking studies of the lead phytochemical, Ulexone B, present in the root of *U. europaeus* (plant), the resulting protein-ligand complex was further investigated using MD simulations to identify its stability and influence on the internal dynamics profile of the 4OR8 receptor. All simulations were carried out with GROMACS 2024.2 for 100 ns using the assisted model building with energy refinement (AMBER) 99 side-chain backbone (SB)-improved leucine, isoleucine, aspartate, asparagine (ILDN) force field (25). Docked complexes were then solved in a dodecahedral box of transferable intermolecular potential with 3 points (TIP3P) water molecules at 1 Å from the complex. Several counterions were added to make the system electrostatically neutral. Long-range electrostatics were treated using Particle Mesh Ewald (PME) and Newton's equations were numerically integrated with a timestep of 2 fs by leapfrog. For the LINCS algorithm, all bonds were constrained. Systems were equilibrated after energy minimisation, 100 ps number of particles, volume, temperature (NVT) and 100 ps number of particles, pressure, temperature (NPT). Production MD was conducted for 100 ns, recording coordinates and velocities every 1 ps. The trajectory analyses were carried out employing the tools included in GROMACS, such as root mean square deviation (RMSD), root mean square fluctuation (RMSF) (by gmx rms and gmx rmsf), radius of gyration (Rg) and solvent-accessible surface area (SASA) (by gmx gyrate and gmx sasa) (Gromacs, 2005). Graphs were generated using XMGrace (v5. 0. 5).

Principal component analysis

Principal component analysis (PCA) was applied to analyse the collective atomic motions using molecular dynamics trajectories. The mass-weighted covariance matrix of atomic positional fluctuations was computed and diagonalised using the gmx covar tool from GROMACS. The eigenvalues describe the atomic motion amplitudes, while the eigenvectors define the directions of the principal components. The obtained principal components were projected onto the molecular dynamic trajectories using gmx anaeig. The cosine content of the principal components was computed using gmx analyse to ensure proper convergence of the PCA. The cosine content of principal component 1(PC1) was found to be less than 0.5, indicating proper convergence and avoiding diffusive motion.

Free energy landscape

The free energy landscapes were computed from the projections along the first and second principal components using gmx sham from GROMACS. The Boltzmann inversion of the two-dimensional probability histogram identifies energy minima as the most stable conformation. Peaks indicate less stable states of the receptors.

Binding free energy

Binding free energy (ΔG_binding) calculations were carried out using the molecular mechanics/Poisson-Boltzmann surface area (MM/PBSA) method and implemented in gmx_MMPBSA. The trajectories of the phytochemical-receptor complex and the phytochemical alone were analysed over 100 ns. The total free energy is partitioned as ΔG_binding = G_complex-(G_receptor + G_phytochemical) and accounts for molecular mechanics, polar solvation using the Poisson-Boltzmann method and the non-polar surface area term.

Results

Protein selection

The protein 4OR8, which shows the crystal structure of MARV VP24, was obtained from the RCSB database (https://www.rcsb.org/) (Fig. 1). The VP24 plays a crucial role in inhibiting interferon signalling by binding to karyopherin α, thereby preventing STAT1 nuclear translocation (26). Other computational studies have also reported the VP24 protein as a potential target for the investigation of an efficient lead molecule against MARV (27).

Molecular docking

Virtual screening has emerged as a powerful tool in modern drug design, enabling the rapid identification of potential drug candidates with high affinities for target proteins or nucleic acids. This was performed to identify potential ligands that could interact with the 4OR8 protein. The PyRx was used to screen a phytochemical library containing 207 compounds. A -7.5 kcal/mol threshold was set based on the most notable negative docking result. Based on the binding energy score, 10 phytochemicals were shortlisted, namely Ulexone B, Ulexone A, Ulexone C, Kaempferol, Oroxylin A, Ursonic acid, Tovoxanthone, 6-Deoxyjacareubin, Warangalone and Ulexone D. These 10 candidates showed high binding affinities of -9.9, -8.7, -8.7, -8, -8, -8, -8, -7.9, -7.9 and -7.9 kcal/mol respectively (Table 1).

Protein-ligand interactivity analysis

The natural compound Ulexone B formed three bonds like conventional hydrogen, π-alkyl and π-sigma with residues Thr A 72 (Thr A chain residue 72), Val A 170 and Val A 170 respectively. Additionally, eight van der Waals forces within proximity were identified with residues Asp A 172, Asn A 171, Val A 169, Asn A 194, Val A 193, Phe A 76, Gln A 71 and Leu A 75. Similarly, for another natural compound, Ulexone A, it also has the same bonds as those of Ulexone B. The Thr A 72 interacts with the ligand via a conventional hydrogen bond and Val A 170 shows Pi-Sigma and Pi-Alkyl interaction. Additionally, Gln A 71, Leu A 75, Phe A 76 and Asn A 194 showed van der Waals forces in proximity (Fig. 2. 1, Fig. 2. 2 and Fig. 2. 3). Further, ADMET analysis was conducted to check the absorption, distribution, metabolism, excretion and toxicity of Ulexone A and Ulexone B. Both compounds ($C_{25}H_{24}O_5$ and $C_{25}H_{22}O_5$, MW ~402–404 g/mol) have good drug-like properties

Table 1. Properties and predicted toxicity class of phytochemicals identified through virtual screening and molecular docking

Compounds	Compound identification number	Binding affinity (kcal/mol)	Molecular weight	Log P	H-Bond acceptors	H-Bond donor	Drug likeness	Toxicity class (as per ProTox 3.0)
Ulexone B	14583601	−9.9	402.45	5.53	5	1	passed	5
Ulexone A	14583600	−8.7	404.46	5.56	5	2	Passed	5
Ulexone C	14583602	−8.7	420.46	4.42	6	2	Passed	5
Kaempferol	5280863	−8	286.05	1.96	6	4	Passed	5
Oroxylin A	5320315	−8	284.27	2.88	5	2	Passed	5
Ursonic acid	9890209	−8	454.7	7.3	2	1	Passed	4
Tovoxanthone	71588335	−8	310.08	2.96	5	2	Passed	5
6-Deoxyjacareubin	5281629	−7.9	310.08	3.1	5	2	Passed	5
Warangalone	5379679	−7.9	404.16	4.38	5	2	Passed	5
Ulexone D	14583603	−7.9	418.45	4.51	6	2	passed	5

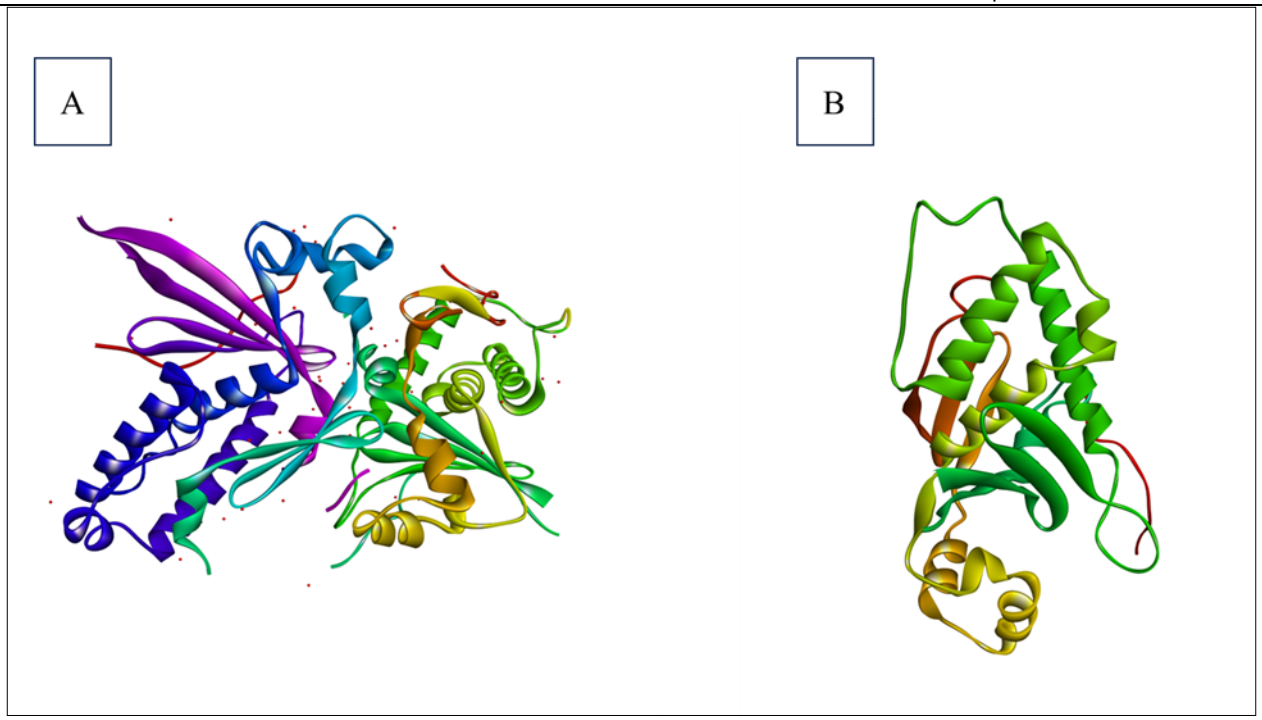


Fig. 1. (A) Unprocessed structure of viral protein 24 (PDB ID: 4OR8); (B) Processed structure of viral protein24 (PDB ID: 4OR8).

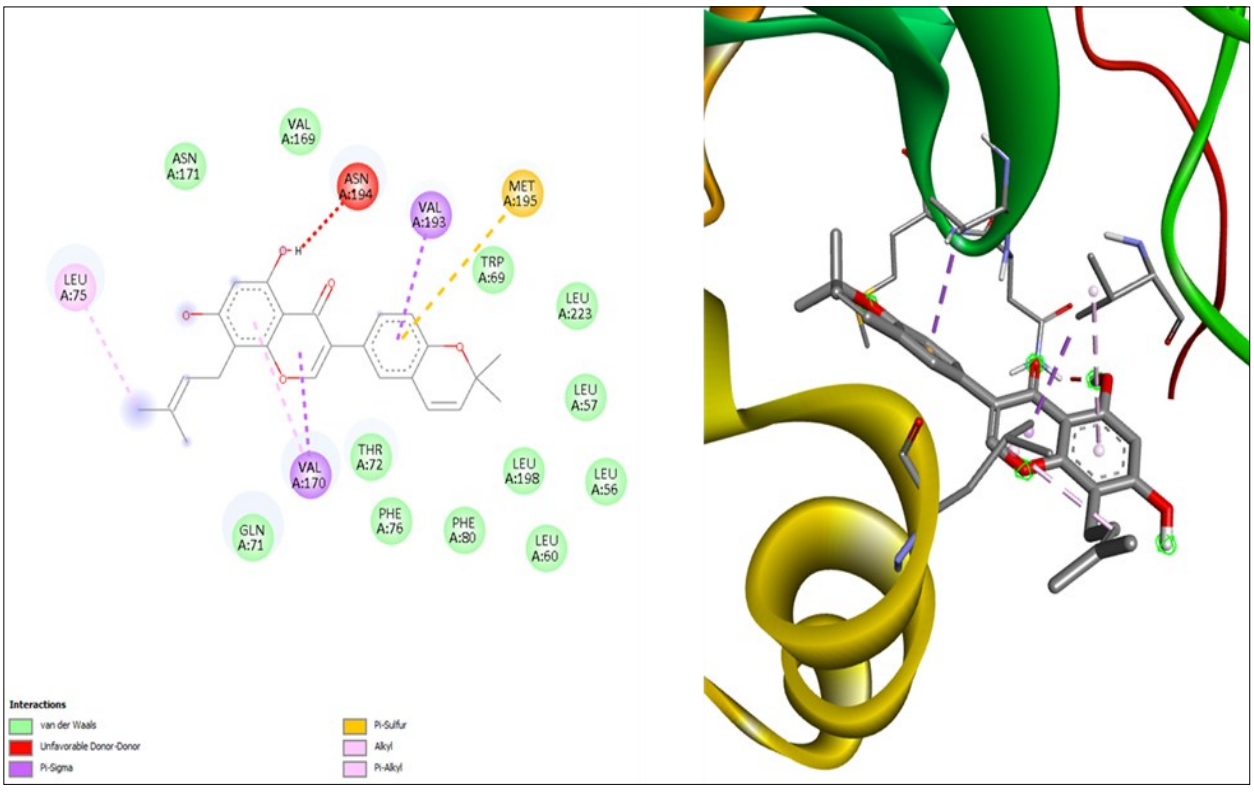


Fig. 2. 1. Ulexone A-2D interaction with the protein viral protein 24 (PDB ID:4OR8).

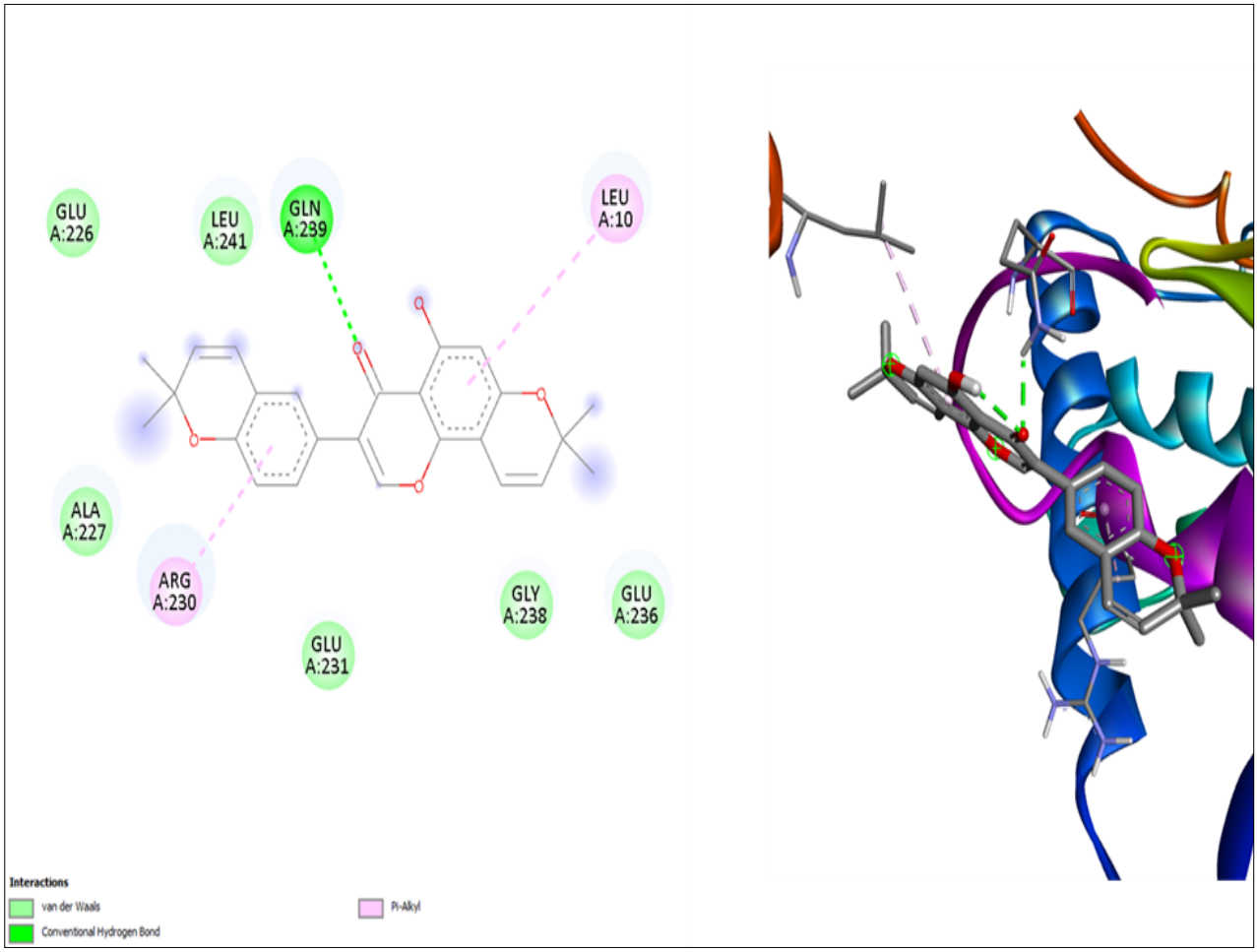


Fig. 2. 2. Ulexone B–2D interaction with the protein viral protein 24 (PDB ID:4OR8).

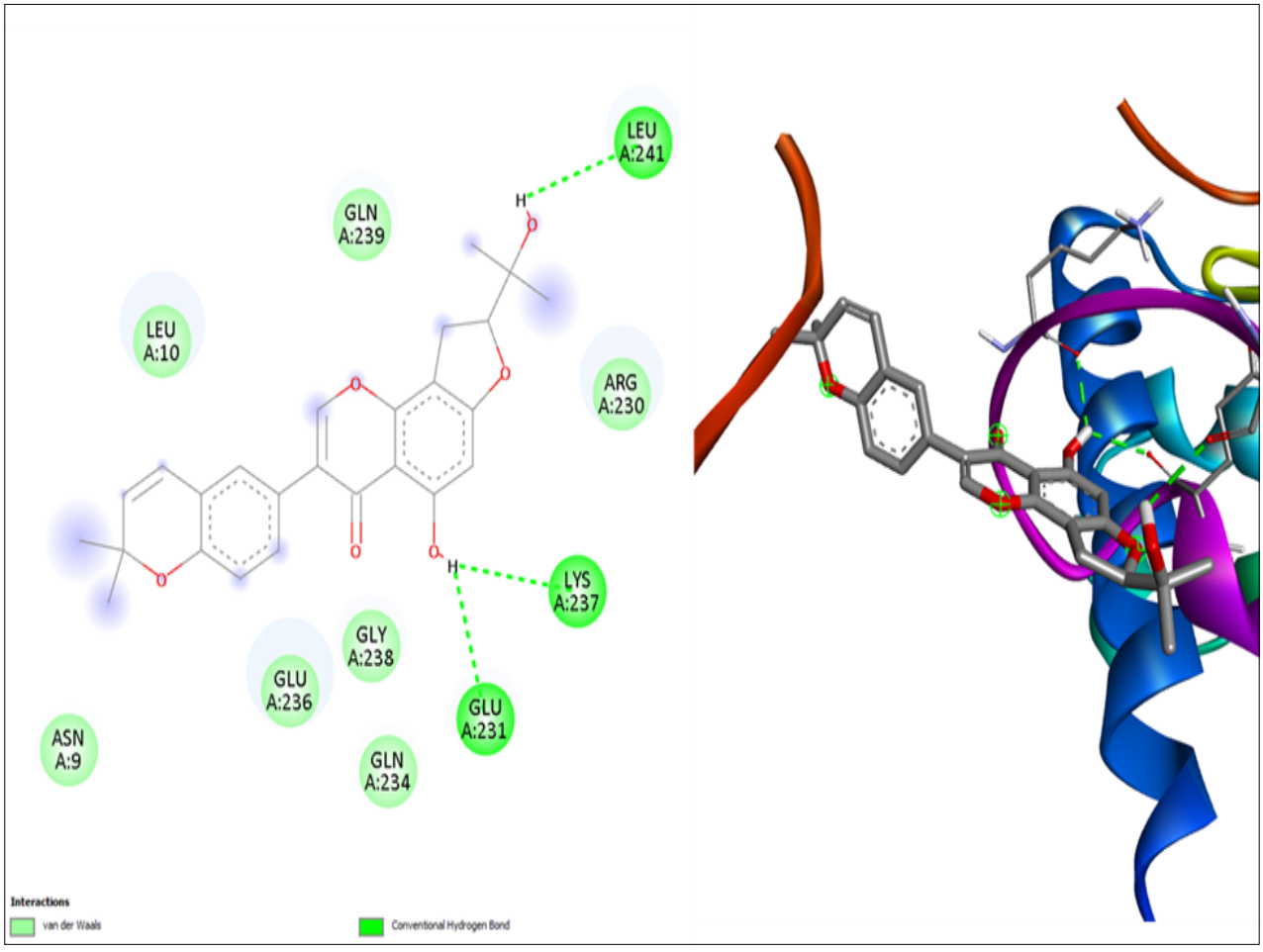


Fig. 2. 3. Ulexone C–2D interaction with the protein viral protein 24 (PDB ID:4OR8).

that satisfy the Lipinski rule of five. They exhibit moderate polarity (TPSA = 68–80 Å^2), low flexibility, high gastrointestinal absorption and moderate bioavailability (score 0.55) (Fig. 3. 1 and Fig. 3. 2). Both compounds reported the toxicity class 4.

Molecular dynamics simulation results

Principal component analysis and free energy landscape analysis

The free energy landscape (FEL) and PCA of the MARV VP24-Ulexone B complex revealed an exceptionally stable structural ensemble. The FEL shows one large global energy minimum (dark purple basin) with its centre at PC1= -2.5, PC2= -2.0, which shows that the system has reached a thermodynamically favourable, stable equilibrium state. Such localised sampling in phase space implies that Ulexone B binding rigidifies the VP24 protein, constraining it with respect to a particular low-energy conformation and reducing the protein's conformational ruggedness compared to its unbound, flexible state. The same stabilisation was observed in the respective RMSD data, which indicated that the structure was equilibrated at 0.45 nm and the RMSF data indicated that the protein core had low variations. Overall, these findings provide good evidence that Ulexone B is a powerful stabiliser of the protein VP24, which probably prevents the change in the manner of conformational transitions essential for the viral activity of this protein (Fig. 4).

Root mean square deviation analysis

The stability of the MARV VP24-Ulexone B complex was determined by computing the RMSD of the C-alpha atoms of proteins over 100 ns. There was an initial peak of significant increase in the RMSD evident in the first 20 ns, to a value close to 0.7 nm, indicating that the complex underwent a significant reorganisation to accommodate the ligand. At 20 ns -80 ns, the system stabilised at a relative plateau with fluctuations of approximately 0.45 nm, indicating structural equilibrium. A secondary deviation occurred at the end of the simulation (85–100 ns) when the RMSD values varied between 0.5 nm and 0.7 nm. These late-stage fluctuations indicate that Ulexone B binding is retained, whereas the VP24 protein has some framework of flexibility (Fig. 5A). The ligand (Ulexone B) RMSD with respect to the protein (VP24) showed variations, which provided insights into the stability of the ligand position in the binding pocket, regardless of the overall movement of the members of the protein complex. The ligand RMSD increased rapidly to a range of 0.5–0.6 nm at the very beginning of the first 5 ns, indicative of the initial equilibration phase, where the ligand changes its position to maximise interactions between the protein residues (Fig. 5B).

Root mean square fluctuation analysis

The profile of the proteins on the RMSF showed that the centre of the VP24 protein was very stable, with the majority of the residues showing low fluctuations of less than 0.2 nm. Flexibility peaks were found at 240 and at the C-terminal region (320–350), where there were significant variations greater than 1.2 nm (Fig. 6). These fluctuating regions probably correspond to flexible loop regions or terminal tails, which are not close to the Ulexone B binding site and the RMSF values are low in other areas, indicating the high structural stability of the binding pocket.

Radius of gyration

The radius of gyration (Rg) was calculated to determine the structural compactness and stability of the Marburg virus VP24-Ulexone B complex. The 100 ns trajectory of the MD simulation was used, as shown in Fig. 7. The Rg profile showed an initial increase between 2.25 nm and 2.45 nm in the first 5–10 ns, due to the equilibration of the system and minor conformational changes as the system bound the ligand. After this, the Rg values stabilised, oscillating in an acceptable range between 2.30–2.50 nm, with an average Rg of 2.40 ± 0.05 nm. These minimal fluctuations suggest a rigid and compact protein-ligand structure, indicating that Ulexone B does not cause significant changes in the interactions with VP24 without inducing a significant unfolding or expansion event.

Analysis of solvent accessible surface area

Further, the analysis of the SASA for the MARV VP24-Ulexone B complex was carried out to assess the solvent exposure and compactness of the complex conformation during the course of the MD simulation trajectory and the results are shown in Fig. 8. The SASA profile showed a rapid decline in the values from 190 nm^2, ranging from 175 to 180 nm^2, in the first few nanoseconds, indicating rapid equilibration, minor adjustments in the conformations and covering of the residues on the surface in the binding interface. After equilibration, around 10 ns, the

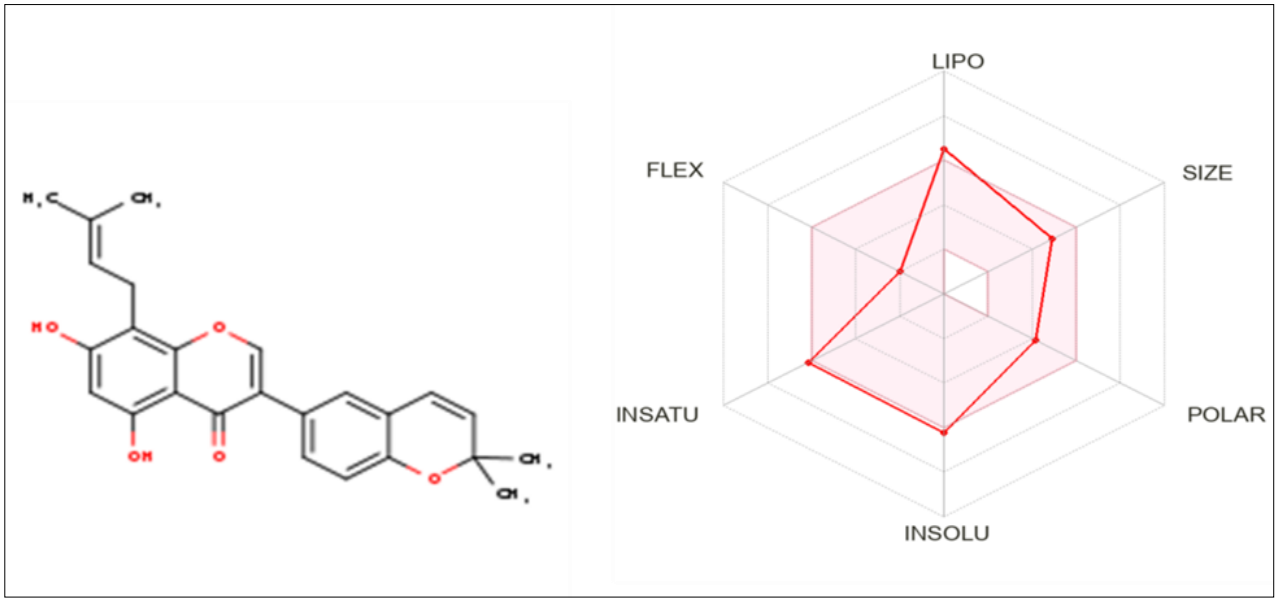


Fig. 3. 1. Swiss absorption, distribution, metabolism and excretion profile of Ulexone A.

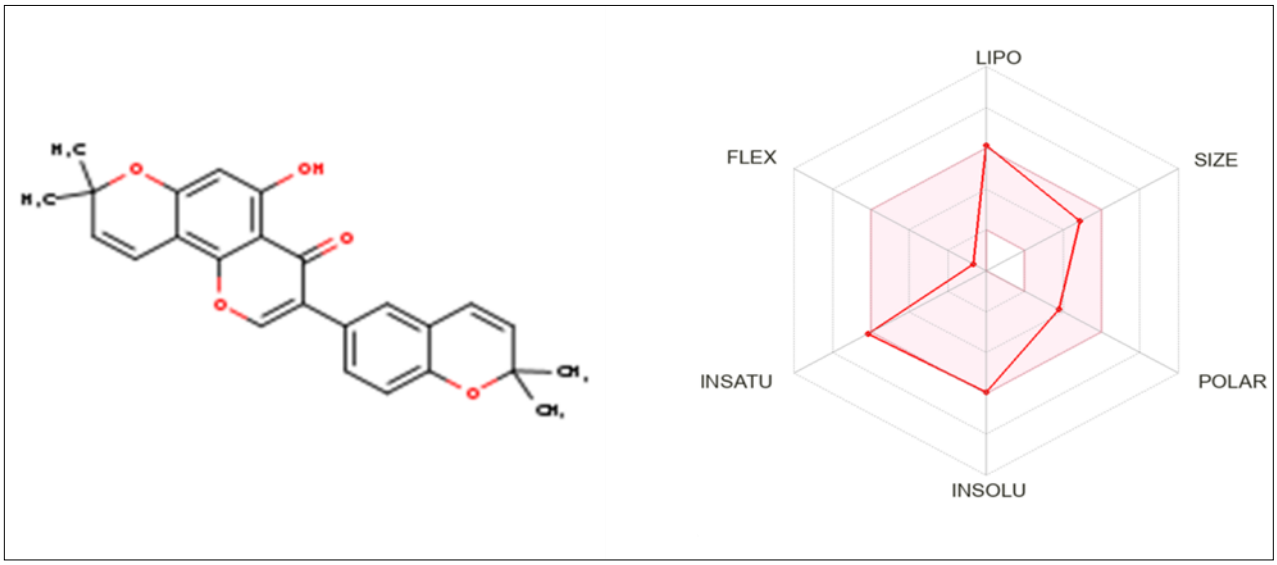


Fig. 3. 2. Swiss absorption, distribution, metabolism and excretion profile of Ulexone B.

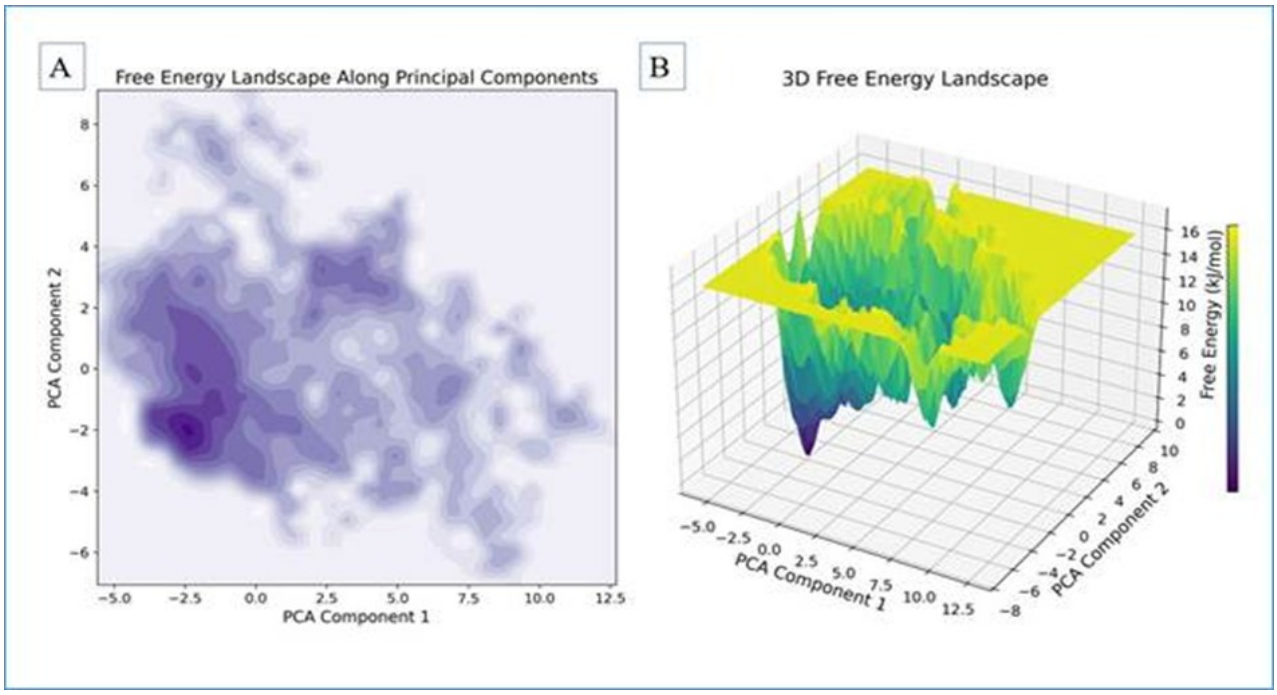


Fig. 4. Free energy landscape of the Marburg virus viral protein 24 -Ulexone B complex. The landscape is projected onto the first two principal components. (A) 2D contour plot; (B) 3D surface map.

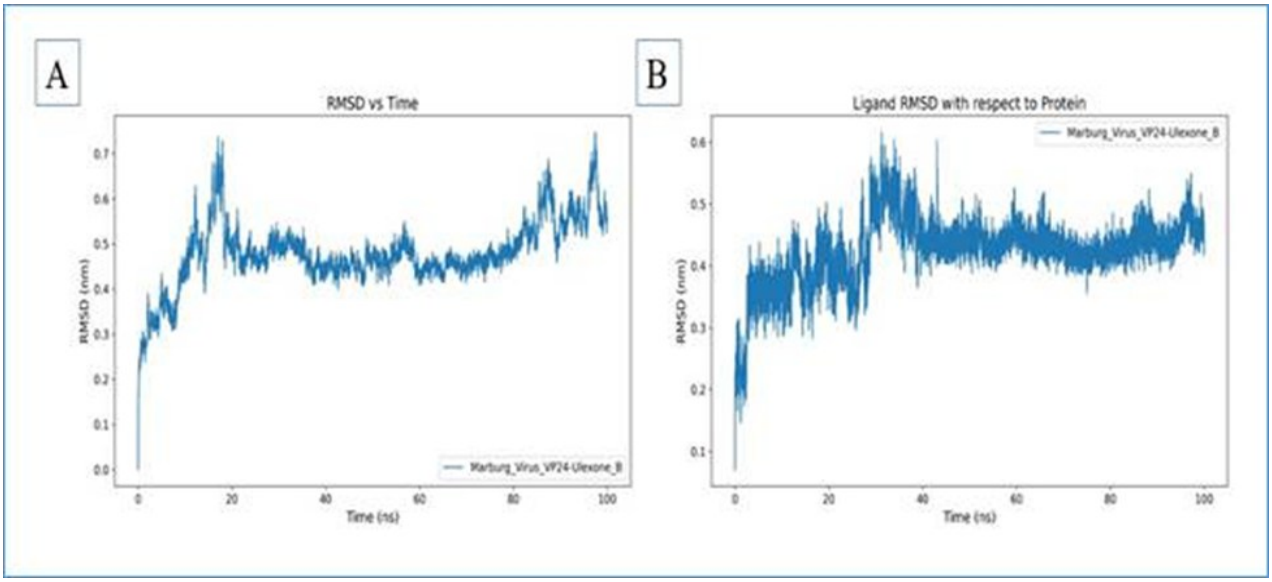


Fig. 5. Root mean square deviation profiles of the Marburg Virus viral protein 24-Ulexone B complex over a 100 ns simulation trajectory (A) Protein root mean square deviation vs time; (B) Ligand root mean square deviation with respect to the protein.

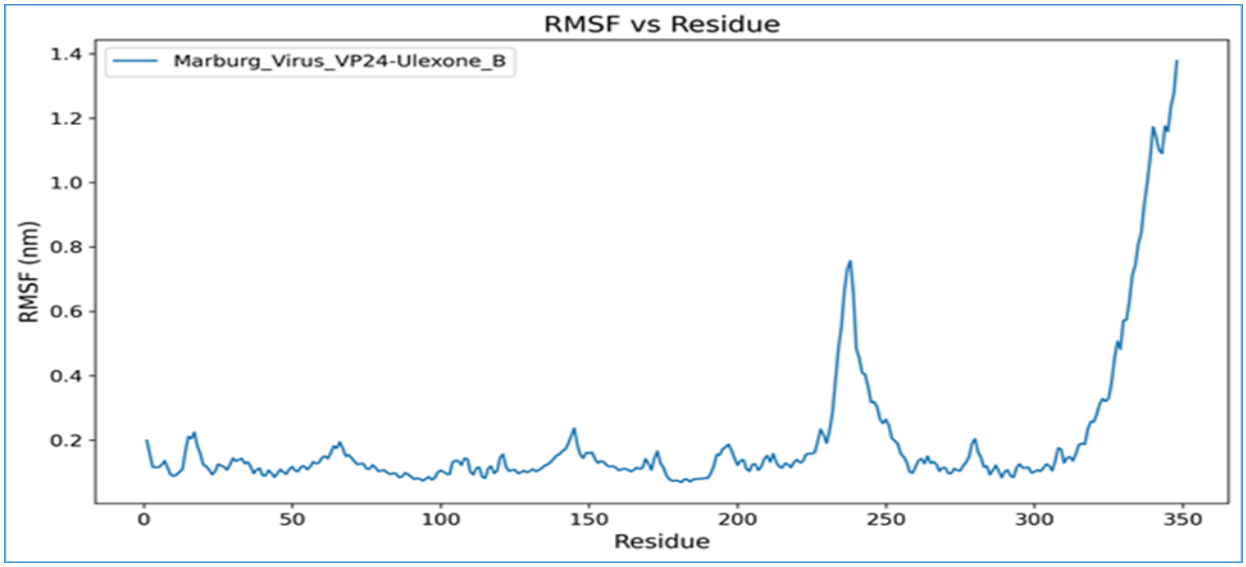


Fig. 6. The root mean square fluctuation plot highlights the local flexibility of individual amino acid residues in the viral protein 24 protein upon binding with Ulexone B.

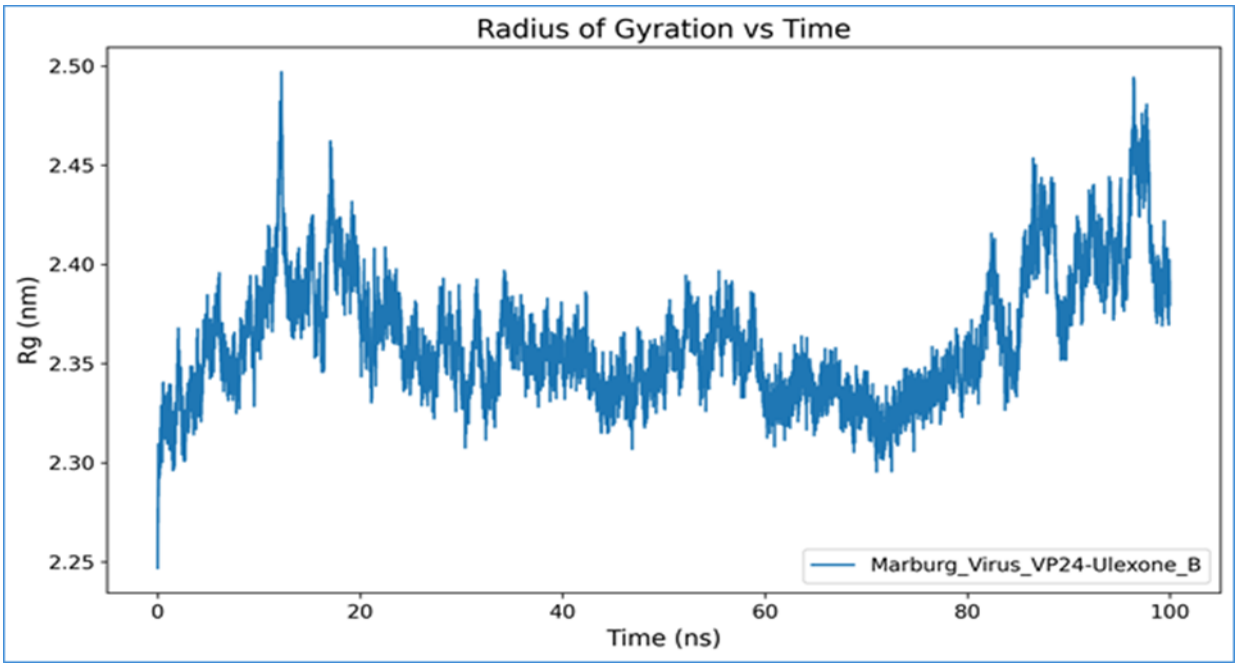


Fig. 7. Radius of gyration trajectory of the Marburg virus viral protein 24-Ulexone B complex at 100 ns molecular dynamics simulation, structural compactness and stability.

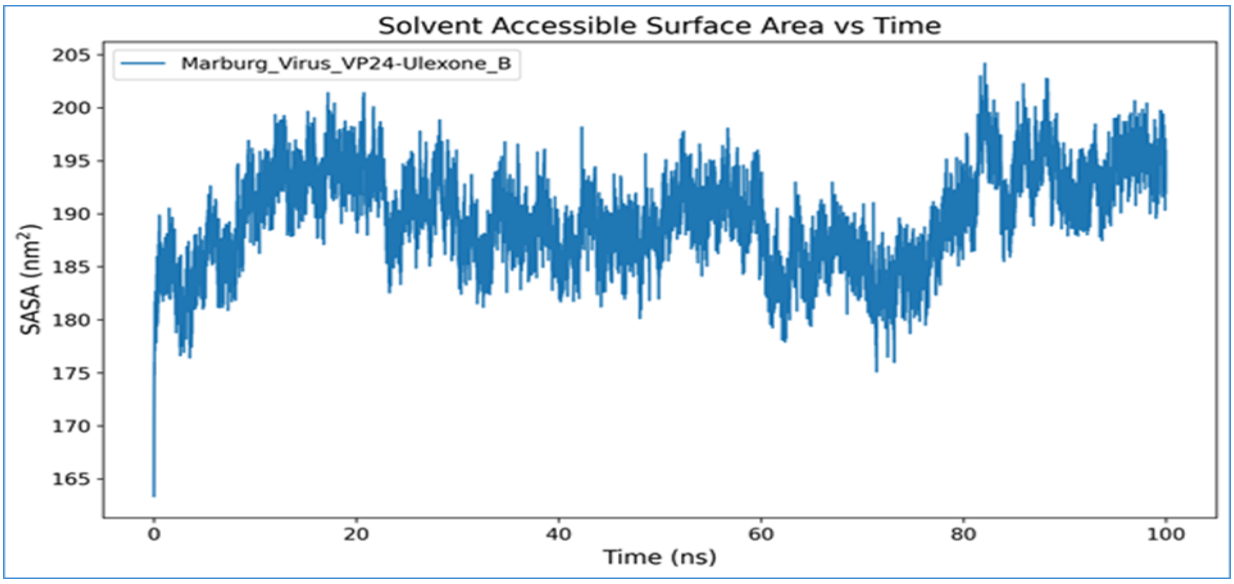


Fig. 8. Time-dependent solvent accessible surface area of the Marburg virus viral protein 24 -Ulexone B complex over 100 ns molecular dynamics simulation, indicating solvent exposure and compactness of the protein-ligand interface.

SASA values ranged from 175 to 205 nm^2, with significant fluctuations in the range from 175 to 185 nm^2 around 50–70 ns and a gradual rise in the range from 195 to 200 nm^2 in the latter part of the trajectory, from 80 to 100 ns. The average SASA value for the equilibrated part of the trajectory, after 10 ns, is found to be around 192 ± 6 nm^2, indicating a limited range of variations or expansions in the trajectory and the changes in the SASA profile indicate that binding with Ulexone B helps in covering some of the exposed regions, leading to a compact interface in the mid-simulation trajectory and the fluctuations in the profile indicate the localised flexibility in the binding pocket. The absence of significant changes in the SASA profile indicates the stability in the conformations, showing no signs of significant unfolding, breaking, or overstretching in the complex.

Hydrogen bond stability

The stability of the protein-ligand interface was also examined through the formation of hydrogen bonds on an orientation basis over time. Within the initial 30 ns of the simulation, the density of polar interactions in the complex was very high, with numerous hydrogen bonds of the complexity maintaining 2–4 hydrogen bonds together. After this period of equilibration, the interaction shifted to a more dynamic phase, determining the interactions between 0 and 2 bonds as the main characteristics of the interaction throughout the rest of the 100 ns (Fig. 9). This tendency implies an elastic binding model with the ligand retained within the pocket through periodic polar contacts, which are probably supported by other noncovalent interactions.

Per-residue energy decomposition

The breakdown of the binding energy per residue was performed to determine the key amino acids that facilitated this interaction. The results showed that there are hotspot residues that play a significant role in stabilising the interaction, such as MET207, THR118, GLY121 and TRP265, which exhibited a significant negative binding energy contribution (Fig. 10). The ligand has a significant role to play and this is clearly demonstrated by its contribution to the energy network. These residues are key targets for structural optimisation because they appear to form a scaffold upon which Ulexone B binds to the MARV VP24 pocket.

Binding free energy calculation (Molecular mechanics/Poisson-Boltzmann surface area method)

To quantify the thermodynamic affinity of the interaction, the binding free energy was estimated by employing the MM/PBSA method. We derived an overall binding energy of -23 kcal/mol, indicating a highly favourable and spontaneous interaction process at a specified concentration. Such stability is brought about through van der Waals interactions (ranging from 0 to 44 kcal/mol) and gas-phase energy (ranging from 0 to 62 kcal/mol). However, a desolvation penalty is derived from a polar solvation energy of + 45 kcal/mol. Nonetheless, a highly negative energy balance is maintained, which indicates a high potency of Ulexone B as an inhibitor (Fig. 11).

Discussion

The present study aimed to investigate the antiviral activity of phytochemicals derived from *U. europaeus* against the MARV VP24 protein by a structure-based virtual screening method and then further validated by molecular dynamic simulations and pharmacokinetic studies. The likelihood of the lead phytochemicals (Ulexone A, B and C) resembling a drug was tested using Lipinski's Rule of Five (Ro5) (Table 2) (Fig. 3.1–3.3). The three compounds qualitatively met the Ro5 criteria since their molecular weights were less than the 500 g/mol threshold, suggesting good oral bioavailability (28). The values of lipophilicity (LogP) and hydrogen bonding capacity (hydrogen bond donors (HBD) and hydrogen bond acceptors (HBA)) also conformed to the recommended ranges (LogP < 5; HBD ≤ 5; HBA ≤ 10), which suggested sufficient aqueous solubility and aqueous membrane permeability (5, 29). These hydrogen bonding properties are essential for stabilisation of protein-ligand complexes and determining binding affinity (30). In addition, the topological polar surface area (TPSA) values of each compound were significantly less than the 140 $Å^2$ trigger, which is a key indicator of effective cell permeation and gastrointestinal absorption (31, 32). Ulexone B was the strongest inhibitor of the screened compounds, with a docking score of -9.9 kcal/mol and stable interactions with VP24 as evidenced by 100 ns MD simulations. Another new antiviral target in filoviruses is VP24, which is a major protein of viral assembly and immune evasion. The hydrogen bond (Thr72) and the hydrophobic interactions (Val170) occurred in Ulexone B, which is a derivative of *U. europaeus* and were supported by the neighbouring amino acids. Ulexone A and C were a little less affine (-8.7 kcal/mol), which means that slight structural variations influence binding. The essential residues that include Met207, Thr118, Gly121 and Trp265 are the ones that indicate a pharmacophoric region that will be utilised in designing future drugs. The 100 ns MD simulations also provided mechanistic information on the dynamic properties of the VP24-Ulexone B complex. The VP24-Cα RMSD converged to a value around 0.45 nm after an initial equilibration period, indicating that the protein maintains

Table 2. Properties of the designed ligands Ulexone A, Ulexone B and Ulexone C that satisfy Swiss absorption, distribution, metabolism and excretion analysis against the target

Properties	Ulexone A	Ulexone B	Ulexone C
Binding affinity (kcal/mol)	−8.7	−9.9	−8.7
Moelcular weight (g/mol)	404.46	402.44	420.45
TPSA (A square)	79.9	68.9	89.13
GI absorption (High = 1; Low = 0)	1	1	1
P-gp substrate (Yes = 1; No = 0)	0	0	1
Log Kp (Skin permeation) (cm/s)	−4.6	−5.05	−5/81
Lipinski	Yes	Yes	Yes
Bioavailability Score	0.55	0.55	0,55
PAIN	0	0	0
Synthetic accessibility	4.22	4.22	4.73

TPSA: Topological polar surface area; GI absorption: Gastrointestinal absorption; P-gp substrate: P-glycoprotein substrate; Log Kp**:** Logarithm of skin permeation coefficient; Lipinski: Lipinski's Rule of Five; PAIN: pan-assay interference compounds.

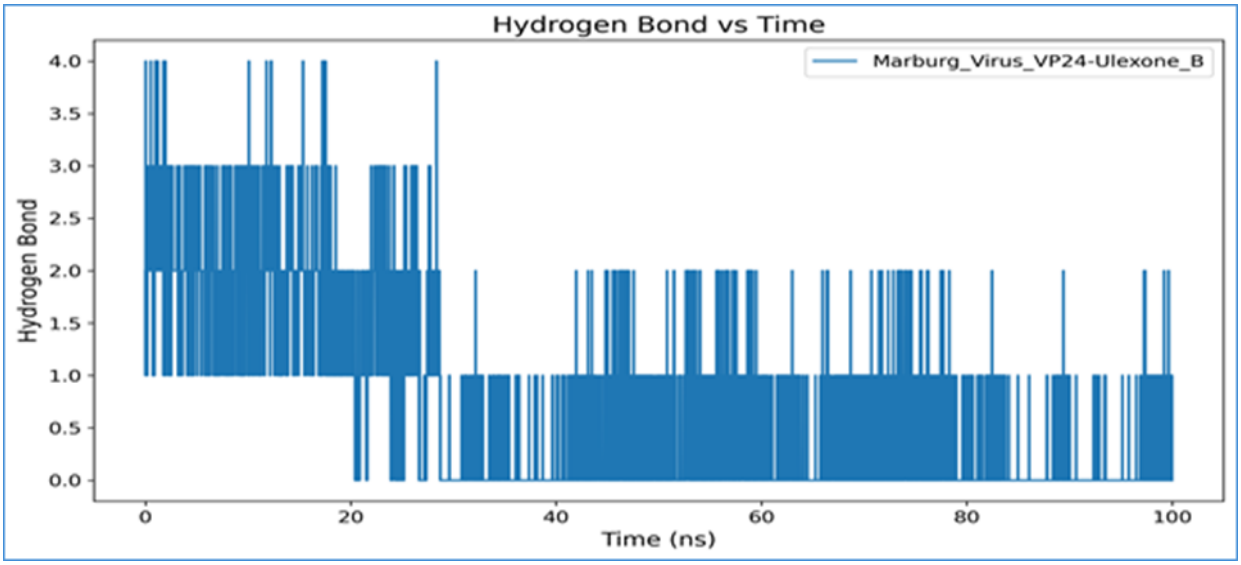


Fig. 9. Intermolecular hydrogen bond profiling.

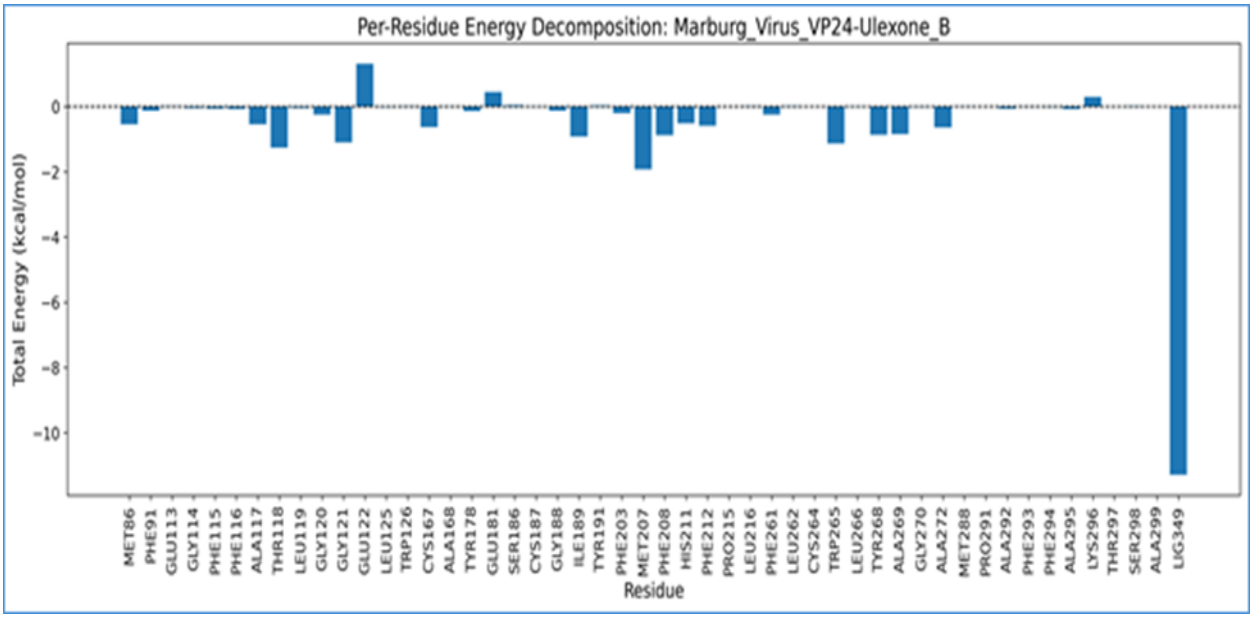


Fig. 10. Per-residue binding energy decomposition.

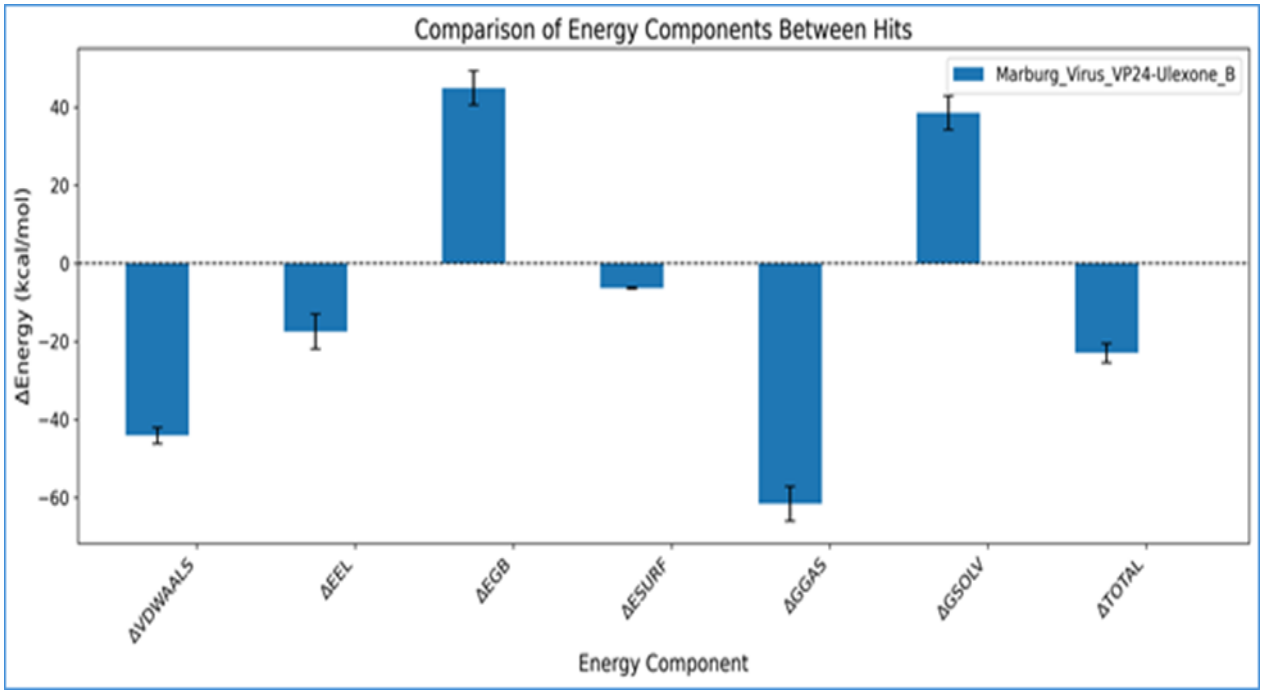


Fig. 11. Comparison of the individual energy components contributing to the total binding affinity of the viral protein 24-Ulexone B complex calculated using molecular mechanics / Poisson-Boltzmann surface area.

a fairly constant shape when bound to Ulexone B and that it retains its structure during the simulation. Analysis of local flexibility via RMSF values indicated that most residues, especially around the interface, showed minimal movements, while larger movements were observed at the terminal and loop regions. This indicates that the binding of Ulexone B does not disrupt VP24 but rather stabilises it into a compact and functionally constrained form. Using ProTox 3.0, the predicted toxicity class for the natural phytochemicals- Ulexone A, Ulexone B and Ulexone C was 5, as shown in Table 3.

The VP24 Ulexone B complex exhibits good binding thermodynamics with an MM/PBSA energy of -23 kcal/mol, which is primarily due to van der Waals and hydrophobic (pi-stacking) interactions with polar solvation penalties compensated by non-polar interactions. The PCA and free energy landscape analysis show that it forms a stable complex with a specific global minimum, indicating limited VP24 conformational flexibility on binding, as it has been previously observed (33–35). General simulation parameters (RMSD, RMSF, Rg, SASA, PCA, FEL) validate the energetic favorability, as well as structural stabilisation.

Its potential is also supported by the ADMET analysis with Ulexone A, B and C meeting Lipinski rule, good membrane permeability and acceptable oral bioavailability. Ulexone B is expected to be low-toxicity (class 5, LD50 ~3850 mg/kg) and has no significant safety concerns, which makes it a promising candidate until it is validated by experiments. This study forms part of the increasing number of *in silico* research endeavours to identify inhibitors against MARV through docking and MD-based methodologies. In a recent study, previous researchers investigated repurposing approved antiviral compounds against MARV targets like VP24 and identified Bictegravir as one of the promising compounds with excellent binding scores and binding free energies (26). Previous researchers identified potential VP40 inhibitors through molecular docking, ADMET analysis and MD simulations and found that their top-ranked compounds have excellent binding stability over long periods of time through MD-based workflows (28).

Filovirus inhibitors are among the natural products that have been identified as useful as antivirals. It has been demonstrated that phytochemicals of *A. paniculata* act as inhibitors of MARV proteins (36). Indonesian natural products have shown inhibitory activity against Ebola VP24 and nucleoprotein with good stability and drug-likeness properties (29, 32). The African-derived compounds have been found to inhibit VP35 to a large extent using integrated computational methods (4). Ulexone B of *U. europaeus*, in this respect, contributes to the list of natural antivirals, which act on MARV proteins. The PCA and free energy surface analysis additionally demonstrate that Ulexone B stabilises VP24 dynamics and sufficient sampling is provided by the first principal component and clear low-energy minima that represent stable conformations. Greater energies represent less desirable conditions, which is in line with prior literature on MARV and Poxviruses that support ligand-stabilised conditions (34). Altogether, the Ulexone B is a promising lead compound because convergence to a stable low-energy state supports it. Despite the valuable input of the current research, it is important to acknowledge certain limitations. First, the study relies entirely on computational predictions, which may not fully capture the complexity of biological systems. This can be resolved by follow-up *in vitro* and *in vivo* validation studies to determine the binding affinity and antiviral properties. Second, the binding energy results and stability calculations rely on the choice of force fields and simulation parameters. Future researchers can use longer simulation times, more force fields and better sampling methods to enhance the accuracy and strength of their results. Third, the single crystal structure (PDB ID: 4OR8) does not consider the variability in conformational changes and strain-specific differences. This can be overcome by using ensemble docking and analysing several protein structures, including mutant forms. Finally, the prediction of pharmacokinetics and toxicity is theoretical and needs to be confirmed by experimental ADMET and toxicity analysis. The mitigation of these drawbacks will greatly increase the reliability and translational capabilities of the lead compound identified. However, the current study is part of and builds upon existing literature that has employed plant-based libraries and computational models to discover potential inhibitors of Marburg proteins, including VP40, VP35 and nucleoprotein. The study focused on a small subset of high-affinity *U. europaeus* plant compounds selected from a large phytochemical library. It also underscores the importance of ethnopharmacologically guided virtual screening strategies. The discovery of Ulexone B as a VP24 ligand with predicted favourable ADMET profiles underscores the importance of *U. europaeus* as a potential source of anti-filoviral compounds that should be systematically explored. In the context of emerging MARV outbreaks and the absence of licensed antiviral and/or vaccines, these leads could serve as starting points for next-generation therapeutic approaches when combined with drug development and virology research efforts.

Conclusion

This study highlights Ulexone B, a phytochemical compound of *Ulex europaeus* L., as a potent *in silico* inhibitor of the Marburg virus viral protein 24. Through a combination of virtual screening, molecular docking and molecular dynamics simulations, Ulexone B demonstrated the highest binding affinity among the tested phytochemicals (-9.9 kcal/mol). It also established strong interactions with the crucial VP24 residues and maintained a stable protein-ligand complex throughout the 100 ns molecular dynamics simulations, as revealed by root mean square deviation, root mean square fluctuation, radius of gyration, solvent accessible surface area, principal component analysis, free energy landscape and molecular mechanics/Poisson–Boltzmann surface

Table 3. Toxicity studies of the selected ligands using ProTox 3.0

Ligands	Predicted LD50 (mg/kg)	Predicted Toxicity Class	Activity of Hepatotoxicity (Active = Yes; Inactive = No)	Activity of Carcinogenicity (Active = Yes; Inactive = No)	Activity of Mutagenicity (Active = Yes; Inactive = No)	Activity of Cytotoxicity (Active = Yes; Inactive = No)
Ulexone A	3850	5	No	No	No	No
Ulexone B	3850	5	No	No	No	No
Ulexone C	3850	5	No	No	Yes	No

area analyses. The *in silico* absorption, distribution, metabolism, excretion and toxicity profile analysis also indicated Ulexone B's drug-likeness and non-toxicity, which differentiates it from its very similar compound Ulexone C. In conclusion, the results of this study place Ulexone B as a promising candidate for further optimisation and experimental validation as a potential anti-Marburg drug targeting VP24. Future studies should confirm the *in silico* predicted antiviral properties of Ulexone B through *in vitro* binding and replication inhibition assays, which determine the impact of VP24 inhibition on the viral life cycle, host interactions and investigate structure-activity relationships through the synthesis of Ulexone B derivatives.

Acknowledgements

The authors would like to thank the University and the supervisor for facilitating and mentoring them throughout the entire research process.

Authors' contributions

SJ performed the literature search, data extraction and analysis, prepared the figures and drafted the original manuscript. DJ performed literature screening and drafted the original manuscript. HAJG contributed to the data validation and assisted in the critical revision of the manuscript. BY assisted in proofreading and the organisation of the pharmacological sections. SPK supervised the entire manuscript and provided critical inputs. PS[1] and MEP reviewed the manuscript for scientific consistency and contributed to abstract refinement. VJU assisted with technical editing and formatting. PS[2] conceptualised the study, supervised the entire project, coordinated communication and prepared the final manuscript draft. All authors read and approved the final manuscript. [PS[1]- P Saranraj, PS[2]-Pallavi Singh]

Compliance with ethical standards

Conflict of interest: Authors do not have any conflict of interest to declare.

Ethical issues: None

Declaration of generative AI and AI-assisted technologies in the writing process

The authors declare that generative AI and AI-assisted technologies were used for language editing, grammar correction and improving clarity. The study utilised computational tools such as PyRx, BIOVIA Discovery Studio, Open Babel, ADMETlab, SwissADME, PyMOL and ProTox-III strictly for research purposes, including molecular docking, visualisation, ligand preparation, validation and toxicity prediction. No AI tools were used for generating, analysing, or interpreting scientific data. After using these tools, the authors reviewed and edited the content as needed and took full responsibility for the content for publication.

References

1. Uppala PK, Karanam SK, Kandra NV, Edhi S. Marburg virus disease: emerging threat, pathogenesis and global public health strategies. World J Virol. 2025;14(2):103576. https://doi.org/10.5501/wjv.v14.i2.103576
2. Srivastava S, Sharma D, Kumar S, Sharma A, Rijal R, Asija A, et al. Emergence of Marburg virus: a global perspective on fatal outbreaks and clinical challenges. Front Microbiol. 2023;14:1239079. https://doi.org/10.3389/fmicb.2023.1239079
3. Letafati A, Fakhr SSH, Najafabadi AQ, Karami N, Karami H. Marburg virus disease: a narrative review. Health Sci Rep. 2025;8(5):e70669. https://doi.org/10.1002/hsr2.70669
4. Abdelrahman AHM, Mekhemer GAH, Sidhom PA, El-Tayeb MA, Khan S, Ibrahim MAA. Exploration of African natural products as VP35 inhibitors to combat Marburg virus infection: molecular docking, molecular dynamics and quantum mechanical computations. PLoS One. 2025;20(10):e0334160. https://doi.org/10.1371/journal.pone.0334160
5. Ramanan P, Shabman RS, Brown CS, Amarasinghe GK, Basler CF, Leung DW. Filoviral immune evasion mechanisms. Viruses. 2011;3(9):1634–49. https://doi.org/10.3390/v3091634
6. Hariprasath R, Akashpriya C, Lakshmaiah VV, Praveen N. In silico studies of viral protein inhibitors of Marburg virus using phytochemicals from *Andrographis paniculata*. J Appl Biol Biotechnol. 2023;11(1):222–31. https://doi.org/10.7324/jabb.2023.110121
7. Carette JE, Raaben M, Wong AC, Herbert AS, Obernosterer G, Mulherkar N, et al. Ebola virus entry requires the cholesterol transporter Niemann-Pick C1. Nature. 2011;477(7364):340–43. https://doi.org/10.1038/nature10348
8. Newman DJ, Cragg GM. Natural products as sources of new drugs over the nearly four decades from 01/1981 to 09/2019. J Nat Prod. 2020;83(3):770–803. https://doi.org/10.1021/acs.jnatprod.9b01285
9. Bakchiche B, Guenane H, Rezzoug M, Gherib A. DPPH free radical scavenging activity of ethanolic extracts of twenty-two medicinal species from South Algeria (Laghouat region). IDOSR J Biochem Biotechnol Allied Fields. 2016;1(1):15–21. https://www.idosr.org/wp-content/uploads/2017/08/IDOSR-JBBAF-11-15-21.pdf
10. Wei YP, Yao LY, Wu YY, Liu X, Peng LH, Tian YL, et al. Critical review of synthesis, toxicology and detection of acyclovir. Molecules. 2021;26(21):6566. https://doi.org/10.3390/molecules26216566
11. Yan XH, Yi P, Cao P, Yang SY, Fang X, Zhang Y, et al. 16-nor limonoids from *Harrisonia perforata* as promising selective 11β-HSD1 inhibitors. Sci Rep. 2016;6:36927. https://doi.org/10.1038/srep36927
12. Nenadovich M, Kubal M, Hopp MR, Crawford AD, Hardewig ME, Sedlock MG, et al. Osage orange (*Maclura pomifera*) and spearmint (*Mentha spicata*) leaf extracts exhibit antibacterial activity and inhibit human respiratory syncytial virus (hRSV). Pathogens. 2025;14(8):776. https://doi.org/10.3390/pathogens14080776
13. Santhi VP, Sriramavaratharajan V, Murugan R, Masilamani P, Gurav SS, Sarasu VP, et al. Edible fruit extracts and fruit juices as potential source of antiviral agents: a review. J Food Meas Charact. 2021;15(6):5181–90. https://doi.org/10.1007/s11694-021-01090-7
14. Bahuguna A, Dubey SK, Garia V, Kumar R, Prakash O, Rawat DS. Composition, antioxidant and anti-inflammatory activities of different polarity extracts of *Anaphalis busua* from the Himalayan terrain of Uttarakhand. Eur J Chem. 2023;14(1):114–120. https://doi.org/10.5155/eurjchem.14.1.114-120.2395
15. Liu L, Liu Y, Yan X, Zhou C, Xiong X. The role of granulocyte colony-stimulating factor in breast cancer development: a review. Mol Med Rep. 2020;21(5):2019–29. https://doi.org/10.3892/mmr.2020.11017
16. Gajurel G, Sharma AR, Abdel-Karim S, Balmaceda C, Zulfiqar F, Pandey P, et al. Enhanced production of anti-inflammatory and antibacterial prenylated isoflavonoids in pigeon pea (*Cajanus cajan*) hairy root cultures. J Agric Food Chem. 2025;73(10):5996–6009. https://doi.org/10.1021/acs.jafc.4c12406
17. BIOVIA, Dassault Systèmes. Discovery Studio Visualizer, version 19.1.0.18287. San Diego: Dassault Systèmes; 2019.
18. Mohanraj K, Karthikeyan BS, Vivek-Ananth RP, Chand RPB, Aparna SR, Mangalapandi P, et al. IMPPAT: a curated database of Indian Medicinal Plants, Phytochemistry and Therapeutics. Sci Rep. 2018;8

(1):4329. https://doi.org/10.1038/s41598-018-22631-z

19. Wang Y, Xiao J, Suzek TO, Zhang J, Wang J, Bryant SH. PubChem: a public information system for analysing bioactivities of small molecules. Nucleic Acids Res. 2009;37(Suppl 2):W623–33. https://doi.org/10.1093/nar/gkp456
20. Sonmez C, Toia B, Eickhoff P, Matei AM, El Beyrouthy M, Wallner B, et al. DNA-PK controls Apollo's access to leading-end telomeres. Nucleic Acids Res. 2024;52(8):4313–27. https://doi.org/10.1093/nar/gkae105
21. Dallakyan S, Olson AJ. Small-molecule library screening by docking with PyRx. Methods Mol Biol. 2015;1263:243–50. https://doi.org/10.1007/978-1-4939-2269-7_19
22. Yadav B, Prasad ME, Upadhye VJ, Kollur SP, Dwivedi A, Singh P. Unravelling the potential of Diospyros species in the treatment of pancreatic adenocarcinoma using an in-silico approach. Plant Sci Today. 2025;12:6346. https://doi.org/10.14719/pst.6346
23. Enmozhi SK, Raja K, Sebastine I, Joseph J. Andrographolide as a potential inhibitor of SARS-CoV-2 main protease: an in-silico approach. J Biomol Struct Dyn. 2021;39(9):3092–98. https://doi.org/10.1080/07391102.2020.1760136
24. Banerjee P, Kemmler E, Dunkel M, Preissner R. ProTox 3.0: a webserver for the prediction of toxicity of chemicals. Nucleic Acids Res. 2024;52(W1):W513–20. https://doi.org/10.1093/nar/gkae303
25. Pronk S, Páll S, Schulz R, Larsson P, Bjelkmar P, Apostolov R, et al. GROMACS 4.5: a high-throughput and highly parallel open-source molecular simulation toolkit. Bioinformatics. 2013;29(7):845–54. https://doi.org/10.1093/bioinformatics/btt055
26. Singh RK, Sarkar K, Das RK. In-silico repurposing of antiviral compounds against Marburg virus: a computational drug discovery approach. *In Silico* Pharmacol. 2025;13(1):41. https://doi.org/10.1007/s40203-025-00323-7
27. Zhang APP, Bornholdt ZA, Abelson DM, Saphire EO. Crystal structure of Marburg virus VP24. J Virol. 2014;88(10):5859–63. https://doi.org/10.1128/JVI.03565-13
28. Das R, Bhattarai A, Tamang B, Thakur N. Identification of potential VP40 inhibitor of Marburg virus through molecular docking, pharmacokinetic analysis and molecular dynamics simulation. Sci Rep. 2025;15(1):27129. https://doi.org/10.1038/s41598-025-12917-4
29. Tambunan USF, Nasution MAF. Identification of novel Ebola virus (EBOV) VP24 inhibitor from Indonesian natural products through in silico drug design approach. AIP Conf Proc. 2017;1862(1):030091. https://doi.org/10.1063/1.4991195
30. Seini A, Ngachilindi Mbeket SB, Fifen JJ, Conradie J. Identification of promising Marburg virus VP24 inhibitors using molecular simulations. ChemRxiv [Preprint]. 2025. https://doi.org/10.26434/chemrxiv-2025-lpfg2
31. Albiheyri R, Ahmad V, Khan MI, Alzahrani FA, Jamal QMS. Investigating the antiviral properties of *Nyctanthes arbor-tristis* Linn against the Ebola, SARS-CoV-2, Nipah and Chikungunya viruses: a computational simulation study. Pharmaceuticals (Basel). 2024;17(5):581. https://doi.org/10.3390/ph17050581
32. Nasution MAF, Toepak EP, Alkaff AH, Tambunan USF. Flexible docking-based molecular dynamics simulation of natural product compounds and Ebola virus nucleocapsid (EBOV NP): a computational approach to discover new drug for combating Ebola. BMC Bioinformatics. 2018;19(Suppl 14):419. https://doi.org/10.1186/s12859-018-2387-8
33. Das R, Bhattarai A, Karn R, Tamang B. Computational investigations of potential inhibitors of monkeypox virus envelope protein E8 through molecular docking and molecular dynamics simulations. Sci Rep. 2024;14(1):19585. https://doi.org/10.1038/s41598-024-70433-3
34. Fu X, Wang Z, Li L, Dong S, Li Z, Jiang Z, et al. Novel chemical ligands to Ebola virus and Marburg virus nucleoproteins identified by combining affinity mass spectrometry and metabolomics approaches. Sci Rep. 2016;6:29680. https://doi.org/10.1038/srep29680
35. Kumar S, Dubey R, Mishra R, Gupta S, Dwivedi VD, Ray S, et al. Repurposing of SARS-CoV-2 compounds against Marburg virus using MD simulation, MM/GBSA, PCA analysis and free energy landscape. J Biomol Struct Dyn. 2025;43(15):8094–8113. https://doi.org/10.1080/07391102.2024.2323701
36. Bhosale S, Kumar A. Screening of phytoconstituents of *Andrographis paniculata* against various targets of Japanese encephalitis virus: an in-silico and in-vitro target-based approach. Curr Res Pharmacol Drug Discov. 2021;2:100043. https://doi.org/10.1016/j.crphar.2021.100043

Additional information

Peer review: Publisher thanks Sectional Editor and the other anonymous reviewers for their contribution to the peer review of this work.

Reprints & permissions information is available at https://horizonepublishing.com/journals/index.php/PST/open_access_policy

Publisher's Note: Horizon e-Publishing Group remains neutral with regard to jurisdictional claims in published maps and institutional affiliations.

Indexing: Plant Science Today, published by Horizon e-Publishing Group, is covered by Scopus, Web of Science, BIOSIS Previews, Clarivate Analytics, NAAS, UGC Care, etc
See https://horizonepublishing.com/journals/index.php/PST/indexing_abstracting

Copyright: © The Author(s). This is an open-access article distributed under the terms of the Creative Commons Attribution License, which permits unrestricted use, distribution and reproduction in any medium, provided the original author and source are credited (https://creativecommons.org/licenses/by/4.0/)

Publisher information: Plant Science Today is published by HORIZON e-Publishing Group with support from Empirion Publishers Private Limited, Thiruvananthapuram, India.